Numerical Methods in Civil Engineering, 9-2 (2024) 29-39

Numerical Methods in Civil Engineering

Journal Homepage: https://nmce.kntu.ac.ir/

Novel SPH and MPS Laplacian Models Improved by MLS Method for Solving Poisson equations

Gholamreza Shobeyri*

ARTICLE INFO

RESEARCH PAPER

Article history:
Received:
June 2024
Revised:
October 2024
Accepted:
November 2024

Keywords:
Mesh-less methods, SPH, MPS,
Improved Laplacian models,
MLS shape functions

Abstract:

The smoothed particle hydrodynamics (SPH) and moving particle semi-implicit (MPS) are well-known and efficient mesh-less numerical methods widely used to investigate a wide range of complicated practical engineering problems. Recently, two modified Laplacian models have been proposed by using different efficient mathematical techniques, and the analogy between SPH and MPS methods. These two models exhibit significantly superior precision in comparison with several existing modified schemes but still suffer from lower accuracy near calculation domain boundaries as they work with the conventional weight or interpolation functions. In this paper, the models were reformulated and further improved by replacing the weight functions with well-known moving least squares (MLS) shape functions without requiring dummy calculation nodes beyond boundaries. The proposed Laplacian models in this study could achieve very accurate results compared with the existing models for the solution of four different two-dimensional Poisson equations on irregular node distributions.

1. Introduction

Numerical methods, in particular mesh-less schemes, have been widely applied to investigate complex and practical engineering problems by solving the corresponding governing differential equations. These methods use a set of calculation nodes with arbitrary configurations to discretize the computational domain and approximate the function value and its derivatives. These methods do not need any computational meshing as a complex and time-consuming process in conventional mesh-based methods, especially in fluid flow simulation using a Lagrangian frame.

Smoothed particle hydrodynamics (SPH) [1] and moving particle semi-implicit (MPS) methods [2] are two efficient and powerful mesh-less approaches with extensive applications in a wide range of engineering problems. In these methods, kernel or weight functions with special properties representing the interaction among calculation nodes are employed to approximate spatial derivatives.

* *Corresponding author: Assistant Professor, Faculty of Civil, Water & Environmental Engineering, Shahid Beheshti University, Tehran, Iran.*
E-mail: g_shobeyri@sbu.ac.ir

SPH and MPS schemes have been successfully developed to simulate complex problems such as landslide waves [3], wave interactions with porous media [4], wave–structure interaction [5], solitary wave interaction with movable seawalls [6], heat transfer [7], lava flows [8], multiphase flows [9], viscous liquid sloshing [10], Ship-wave Interactions [11], mass transfer mechanisms of rotary atomization [12], and bubble dynamics in sodium [13].

Several studies have been conducted on the development of SPH and MPS methods in recent years. Low approximation accuracy due to particle inconsistency in SPH has been addressed by retaining the conventional non-negative smoothing function [14]. A new renormalization-based formulation in the context of the SPH method was proposed to solve the Euler equations [15]. A more accurate SPH Laplacian model was obtained by using a gradient term calculated from Taylor series expansion in the classic SPH formulations [16]. To achieve a smoother pressure field in modeling liquid sloshing dynamics, a kernel gradient correction was introduced for the SPH method [17]. A mixed corrected symmetric SPH approach was introduced and

https://doi.org/10.61186/NMCE.2406.1061

applied to solve and simulate the non-linear dynamic problems and fluid flows [18]. A corrected higher-order Laplacian model obtained from the divergence of a modified SPH gradient model was employed to solve ocean engineering applications [19]. Huang et al. [20] applied a novel SPH Laplacian model by using a kernel gradient-free approach to study incompressible fluid flows. Zhu et al. [21] introduced an efficient multiphase interface treatment scheme coupled with a dynamic boundary treatment approach to improve the numerical performance of SPH in the simulation of multiphase flows. To examine the smoothing error in SPH operators, a comprehensive study was conducted by Violeau and Fonty [22]. Several SPH Laplacian models had their accuracies enhanced by the so-called Voronoi diagram to estimate calculation node volume [23]. Heydari et al. accomplished an extensive accuracy analysis of several modified Laplacian SPH schemes [24]. Two new TSE-based SPH gradient and Laplacian models were formulated to study free surface problems and convection heat transfer [25]. A new inverse logarithmic kernel function was proposed to enhance the accuracy of the SPH method [26]. A hybrid high-order SPH scheme based on the MLS approximation was recently established to more efficiently simulate compressible flows with discontinuities [27]. Irregular nodal distribution which is a challenging issue for the SPH method was amended using efficient particle shifting techniques [28-29]. Several similar research studies have also been carried out to amend the intrinsic drawbacks of the MPS method [30-38].

A significant shortcoming of SPH and MPS methods is the low accuracy of their conventional weight functions. These functions can cause large errors primarily due to irregular node distributions, the shape of the computational domain, and the lack of calculation nodes beyond the boundaries. A simple yet relatively inefficient approach to solving these problems is the use of dummy particles in areas beyond the computational domain, whose arrangement is complicated for complex geometries. Recently, two improved SPH and MPS Laplacian models [39, 40], based on weight functions, have been proposed using efficient mathematical approaches, achieving remarkable accuracy compared with several existing modified models [2, 16, 20, 41-44]. However, these methods still suffer from the problems mentioned above. To amend the shortcomings, moving least squares (MLS), a well-known scheme in function approximation can be used instead of weight functions in a way that is compatible with the formulations of the improved models. Compared with their original forms, the proposed schemes can get much more accurate results for several Poisson equations on complex geometries with no need for dummy nodes. Accordingly, these models can be successfully applied to complex problems encountered in fluid and solid mechanics.

2. Mesh-less models

This section presents the fundamental formulation of the considered mesh-less schemes, including MLS, SPH, and MPS methods. In addition, the proposed mixed formulation coupled with the MLS scheme is used to reduce the order of the governing partial differential equations (PDEs), followed by verifying the expected higher accuracy of the introduced methods over the existing models.

2.1 MLS method

The value of an arbitrary function (f) can be evaluated using the MLS scheme as follows:

$$f(\mathbf{x_a}) = \sum_{i=1}^{m} p_i(\mathbf{x})\, a_i(\mathbf{x}) \equiv \mathbf{p}^T(\mathbf{x})\, \mathbf{a}(\mathbf{x}) \tag{1}$$

where m gives the number of terms in the polynomial basis functions, $\mathbf{p}^T(\mathbf{x})$ is a monomial basis and $\mathbf{a}(\mathbf{x})$ represents a vector of unknown values. For two-dimensional problems, the following equations express the polynomial basis [45].

$$\begin{aligned} &\mathbf{P} = 1 && \text{for } m\text{=}1 \\ &\mathbf{P} = [1\ x\ y]^T && \text{for } m\text{=}3 \\ &\mathbf{P} = [1\ x\ y\ x^2\ xy\ y^2]^T && \text{for } m\text{=}6 \end{aligned} \tag{2}$$

where x and y are the components of the Cartesian coordinates. It should be noted linear polynomial basis (m=3) is used for the computations in this study.

The sum of the weighted squared residuals (J) is defined as:

$$J = (\mathbf{P}.\boldsymbol{\alpha}(\mathbf{x}) - \mathbf{f})^T.\mathbf{W}.(\mathbf{P}.\boldsymbol{\alpha}(\mathbf{x}) - \mathbf{f}) \tag{3}$$

The vector of unknown values ($\mathbf{a(x)}$) is obtained by minimizing the function J as:

$$\boldsymbol{\alpha}(\mathbf{x}) = \mathbf{A}^{-1}(\mathbf{x}).\mathbf{B}(\mathbf{x}).\mathbf{u} \tag{4}$$

In the above equation, $\mathbf{f}^T = (f_1, f_2, ..., f_n)$, $\mathbf{A}(\mathbf{x}) = \mathbf{P}^{\mathbf{T}}.\mathbf{W}.\mathbf{P}$, $\mathbf{B}(\mathbf{x}) = \mathbf{P}^{\mathbf{T}}.\mathbf{W}$ and $\mathbf{W}$ is the value of the weight function:

The unknown function $f(\mathbf{x})$ can be expressed as follows:

$$f(\mathbf{x}) = \sum_{i=1}^{n} N_i(\mathbf{x}).f_i \tag{5}$$

where $N_i(\mathbf{x})$ is the shape function of the node i given by:

$$N_i(\mathbf{x}) = \mathbf{p}^T(\mathbf{x})\ \mathbf{A}^{-1}(\mathbf{x}).\mathbf{B}(\mathbf{x}) \tag{6}$$

A promising feature of this function is the unity property expressed by the following equation:

$$\sum_{i=1}^{n} N_i(\mathbf{x}) = 1 \tag{7}$$

This property is achieved for arbitrary calculation node

distributions, leading to notable accuracy in function estimation even near computational domain boundaries.
Finally, the derivatives of the MLS shape function are obtained by:

$$\frac{\partial N}{\partial x}=\frac{\partial \mathbf{p}^T}{\partial x}\ \mathbf{A}^{-1}\mathbf{B}+\mathbf{p}^T\frac{\partial \mathbf{A}^{-1}}{\partial x}\ \mathbf{B}+\mathbf{p}^T\mathbf{A}^{-1}\frac{\partial \mathbf{B}}{\partial x} \tag{8}$$

$$\frac{\partial N}{\partial y}=\frac{\partial \mathbf{p}^T}{\partial y}\ \mathbf{A}^{-1}\mathbf{B}+\mathbf{p}^T\frac{\partial \mathbf{A}^{-1}}{\partial y}\ \mathbf{B}+\mathbf{p}^T\mathbf{A}^{-1}\frac{\partial \mathbf{B}}{\partial y} \tag{9}$$

Using these equations, the first derivatives of the unknown function can be evaluated by:

$$\frac{\partial f}{\partial x}=\sum_{i=1}^{n}\frac{\partial N_i(\mathbf{x})}{\partial x}.f_i \tag{10}$$

$$\frac{\partial f}{\partial y}=\sum_{i=1}^{n}\frac{\partial N_i(\mathbf{x})}{\partial y}.f_i \tag{11}$$

As powerful mesh-less approaches, SPH and MPS have found many applications in various complex engineering problems. Several modifications, including those explained in Section 1, have been proposed to improve these methods and amend their inherent deficits. MLS-modified SPH and MPS are presented in the following subsections, and discussions are given on their effectiveness.

2.2 SPH method

In the standard SPH method, the theory of integral and weight functions is applied to approximate an arbitrary field function and the corresponding gradient and Laplacian operators based on the following equations, respectively [41]:

$$f(\mathbf{r}_a)=\sum_{\mathrm{b}} f(\mathbf{r}_b)W_{ab}\Delta V_{\mathrm{b}} \tag{12}$$

$$\nabla f_a=\sum_{\mathrm{b}}(f_b-f_a)\nabla W_{\mathrm{ab}}\Delta V_b \tag{13}$$

$$\nabla^2 f_a=\sum_{b}\frac{-2\mathbf{r}_{ab}.\nabla W_{ab}}{|\ \mathbf{r}_{ab}\ |^2}(f_b-f_a)\Delta V_b \tag{14}$$

$$\frac{1}{\Delta V_a}=\sum_{b}\frac{1}{\Delta V_b}W_{\mathrm{ab}}\Delta V_b=\sum_{b}W_{\mathrm{ab}}\rightarrow \Delta V_a=\frac{1}{\sum\limits_{b}W_{\mathrm{ab}}} \tag{15}$$

where *a* is the reference node, *b* denotes neighbor nodes of node *a*, $\mathbf{r}$ is the position vector, W_{ab} gives the value of weight function, and ΔV is also the node volume.
A common weight function of the SPH method is as follows:

$$W(r=|\mathbf{r}_{\mathrm{a}}-\mathbf{r}_b|,R_s)=W_{ab}=\frac{8}{\pi R_s^2}\left(\frac{3}{4}\left(\frac{r}{R_s}\right)^2-\frac{3}{2}\left(\frac{r}{R_s}\right)+\frac{3}{4}\right) \tag{16}$$

where R_s is the radius of the interaction area of the reference node.

The unity property of the SPH weight function in continuous form can be expressed by:

$$\int_{\Omega}W(r,R_s)dr=1 \tag{17}$$

The discrete form of the weight functions applied in SPH calculation does not possess the unity property, leading to low accuracy of the method, especially near boundaries where no calculation nodes exist beyond the computational domain.

2.3 MPS method

Using a weighted average scheme in the MPS method, the gradient and Laplacian operators can be formulated as follows [2]:

$$\nabla f_a=\sum_{b\neq a}\frac{d}{n_b}\frac{f_a-f_b}{|\ \mathbf{r}_a-\mathbf{r}_b\ |^2}(\mathbf{r}_a-\mathbf{r}_b)W_{ab} \tag{18}$$

$$\nabla^2 f_a=\frac{2d}{\lambda}\sum_{b\neq a}\frac{1}{n_b}(f_b-f_a)W_{ab} \tag{19}$$

where d is the number of dimensions, and n_b and are λ two computational parameters defined by the following equations, respectively.

$$n_a=\sum_{b\neq a}W_{ab} \tag{20}$$

$$\lambda=\frac{\int_{\Omega}W(r)r^2d\Omega}{\int_{\Omega}W(r)d\Omega} \tag{21}$$

where Ω is the influence area of the considered node and r also is distance of the calculation nodes.
The MPS method like SPH uses the discrete form of weight functions and its precision decreases near calculation domain boundaries.

2.4 Improved SPH method

Considering the similarity between equations (13) and (14), the standard SPH Laplacian model can be rewritten as:

$$\nabla^2 f_a=\sum_{b}\frac{-2\mathbf{r}_{ab}.(Cof\_Grad)(f_b-f_a)}{|\ \mathbf{r}_{ab}\ |^2} \tag{22}$$

In the above equation, Cof_Grad is the coefficient of a gradient model having a similar form to that of the standard SPH model (equation (13)). It has been shown that SPH and MPS methods can be combined because of their analogy, to derive novel improved models. Recently, a modified Laplacian model with significant accuracy has been introduced by coupling these methods as follows:

$$\nabla^2 f_a = \sum_b \frac{-2\mathbf{r}_{ab}.(Cof\_Grad\_MPS)(f_b - f_a)}{|\mathbf{r}_{ab}|^2} \quad (23)$$

where, Cof_Grad_MPS can be expressed by:

$$Cof\_Grad\_MPS = [\frac{1}{\lambda}\sum_{b\neq a}\frac{1}{n_b}W_{ab}(\mathbf{r}_b - \mathbf{r}_a)\otimes(\mathbf{r}_b - \mathbf{r}_a)^T]^{-1}$$
$$[\frac{1}{\lambda}\sum_{b\neq a}\frac{1}{n_b}W_{ab}(\mathbf{r}_b - \mathbf{r}_a)] \quad (24)$$

where $\otimes$ refers to the cross-product. More details of this model can be found in a related study [39].

As explained before, MLS is a highly accurate scheme for approximating a field function, which makes it an alternative to the weight function in the above equations. In other words, equation (24) is modified as:

$$Cof\_Grad\_MPS = [\frac{1}{\lambda}\sum_{b\neq a}N_{ab}(\mathbf{r}_b - \mathbf{r}_a)\otimes(\mathbf{r}_b - \mathbf{r}_a)^T]^{-1}$$
$$[\frac{1}{\lambda}\sum_{b\neq a}N_{ab}(\mathbf{r}_b - \mathbf{r}_a)] \quad (25)$$

where N_{ab} is the value of the MLS function of the node a at the location of node b. To derive the above equation, the unity property of the MLS functions and the corresponding expression in the MPS formulations based on equation (20) give the following:

$$N_{ab} \approx W_{ab} / \sum n_b \quad (26)$$

2.5 Improved MPS method

A novel 2D Laplacian MPS model exhibiting promising accuracy has been recently formulated by taking the divergence of the improved MPS model described by the following equation [40]:

$$\nabla^2 f_a = \frac{1}{\lambda}(ar_{11} + ar_{22})\left[\sum_{b\neq a}\frac{1}{n_b}W_{ab}(f_b - f_a)\right]) \quad (27)$$

In the above equation, ar_{11} and ar_{22} are the arrays of the main diagonal of a 2 by 2 corrective matrix (the right-hand side of equation (28)) defined by:

$$\begin{bmatrix} ar_{11} & ar_{12} \\ ar_{21} & ar_{22} \end{bmatrix} = [\frac{1}{\lambda}\sum_{b\neq a}\frac{1}{n_b}W_{ab}(\mathbf{r}_b - \mathbf{r}_a)\otimes(\mathbf{r}_b - \mathbf{r}_a)^T]^{-1} \quad (28)$$

The accuracy of this Laplacian model can be enhanced using the same approach introduced for the proposed SPH Laplacian model (See equation (26)) in the previous sub-section as follows:

$$\nabla^2 f_a = \frac{1}{\lambda}(ar_{11} + ar_{22})\left[\sum_{b\neq a}N_{ab}(f_b - f_a)\right]) \quad (29)$$

In the above model, the calculation of the inverse of the corrective matrix and the mathematical operations of MLS functions slightly increase the computational cost.

2.6 Mixed formulation

Let a system of first-order differential equations be expressed by the following equations:

$$A^x\frac{\partial F}{\partial x} + A^y\frac{\partial F}{\partial y} + A^0 F = S \quad (30)$$

where F, S, A^x, A^y, and A^0 are defined as follows :

$$F = [f, f_x, f_y]$$
$$S^T = [0, 0, g(x,y)]$$
$$A^x = \begin{bmatrix} 1 & 0 & 0 \\ 0 & 0 & 0 \\ 0 & a_x & c_{xy} \end{bmatrix}$$
$$A^y = \begin{bmatrix} 0 & 0 & 0 \\ 1 & 0 & 0 \\ 0 & 0 & b_y \end{bmatrix}$$
$$A^0 = \begin{bmatrix} 0 & -1 & 0 \\ 0 & 0 & -1 \\ 0 & 0 & 0 \end{bmatrix} \quad (31)$$

Here, the vector F includes a function (f) and its derivatives (f_x, f_y). In addition, a_x, b_y and c_{xy} are arbitrary coefficients and $g(x,y)$ is a field function.

By multiplying the matrixes (A^x, A^y and A^0) into the vectors (F, $\partial F/\partial x$ and $\partial F/\partial y$) in the above equations, the flowing second-order PDE is derived:

$$a_x\frac{\partial^2 f}{\partial x^2} + b_y\frac{\partial^2 f}{\partial y^2} + c_{xy}\frac{\partial^2 f}{\partial x\partial y} = g(x,y) \quad (32)$$

In numerical mathematics, approximation of second-order derivatives with acceptable accuracy is difficult. To avoid this expensive process, a mixed formulation has been widely applied in which a system of first-order differential equations (equation (29)) is used instead of the second-order PDE (equation (32)) [46, 47]. By assuming $a_x = b_y$ and $c_{xy} = 0$, a 2D Poisson equation can be derived. The desired PDE (equation (30)) with the unknown vector F can be discretized by approximating functions F and their derivatives ($\partial F/\partial x$ and $\partial F/\partial y$) using the corresponding MLS formulations (equations (5, 10, and 11), respectively). After solving the corresponding equations, the values of the unknown vector are determined, and its first component

represents the considered unknown function (f) of equation (32). This scheme has been successfully applied for the discrete least squares meshless (DLSM) method for simulating fluid flows [48, 49].

3. Numerical case studies

In this section, four Poisson equations are considered to examine the numerical performance of the proposed Laplacian models briefly explained in Table 1. The PDEs are given in the following equations:

Equation A : $\nabla^2 f = 6x\sin(2\pi y) + 4\pi^2\sin(2\pi y)(x - x^3)$

Exact solution: $f = (x^3 - x)\sin(2\pi y)$ (33)

Equation B : $\nabla^2 f = 2(y^3 - y) + 6y(x^2 - x)$

Exact solution: $f = (x^2 - x)(y^3 - y)$ (34)

Equation C : $\nabla^2 f = 6xy^2 + 2(x^3 - 1)$

Exact solution: $f = (x^3 - 1)y^2$ (35)

Equation D : $\nabla^2 f = -128\pi^2\cos(8\pi y)\sin(8\pi x)$;

Exact solution: $f = \sin(8\pi x)\cos(8\pi y)$ (36)

Table 1: The evaluated Laplacian models in this study

Name	Given by	Description
Model 1	Equations (22-24)	The improved SPH model proposed in Ref. [39].
Model 2	Equation (25)	The modified version of Model 1 using the MLS shape function.
Model 3	Equation (27)	The improved MPS model proposed in Ref. [40].
Model 4	Equation (29)	The modified version of Model 3 using the MLS shape function.
Model 5	Equations (30-32)	The mixed model with MLS shape function.

To solve the PDEs, several irregular node distributions were used for the Laplacian models. The nodes were initially arranged into a uniform square grid with spacing L_0 and then they were redistributed using a random number generator (see figure 1). To solve the first PDE (equation (33)), $L_0 = 1/20$ m, $1/30$ m, $1/40$ m was applied and the corresponding numerical errors (Er) of the models were plotted (see figure 2). The error of the numerical results is defined as the mean errors of the calculation nodes regarding the available exact solution of the differential equations. It should be noted that the numerical errors of the models can be slightly variable in different runs due to random distributions of calculation nodes.

As seen in figure 2, Models 2 and 4 can get higher accuracy levels than their original forms (*i.e.*, improved versions of Models 1 and 3, respectively), demonstrating the efficiency of incorporating the MLS shape function into the original models. From the results, all SPH and MPS models, especially the proposed models in this study, realized smaller errors than the mixed MLS model (Model 5) as a classic approach to solving second-order PDEs. Despite their better results in terms of error compared to the classic SPH and MPS methods [39, 40], Models 1 and 3 require at least one extra node layer beyond the boundaries to get acceptable precision. This can be explained by the fact that the models accomplish function estimation using the discrete kernel functions with no unity property. On the other hand, the proposed models in this study (MLS-modified Models 2 and 4) can achieve higher accuracy with no need for any additional node layer beyond the boundaries. The numerical solution obtained from Model 2 is illustrated in figure 3, and the solution along $x = 0.5$ m is compared with the exact results, exhibiting promising agreement as shown in figure 4. Thanks to the availability of the analytical solution, the values of the unknown function of the considered differential equation were determined at the boundary nodes and then directly applied in calculations as Dirichlet boundary conditions. Neither MLS nor kernel functions satisfy the Kronecker delta property, so imposing boundary conditions with this simple scheme may introduce small errors in computations. More accurate approaches such as Lagrange multipliers [50] and penalty methods [51] can also be used to impose the boundary conditions. In addition, different approaches have been proposed to satisfy the Kronecker delta property for MLS functions [52-54].

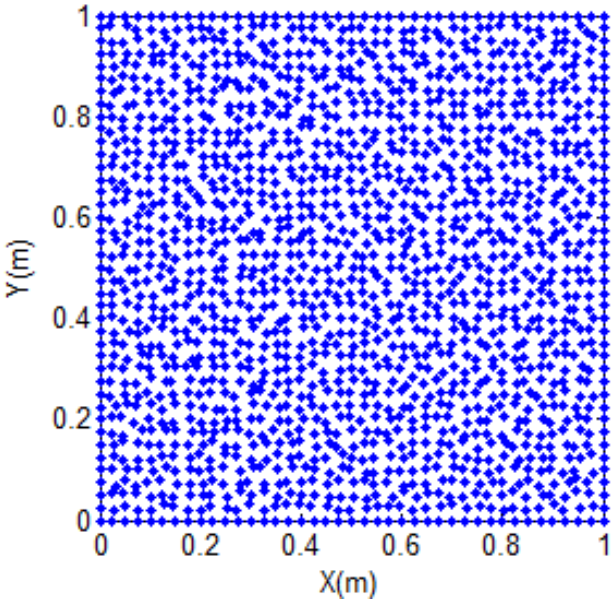

Fig. 1: A sample calculation node configuration with $L_0 = 1/40$ m.

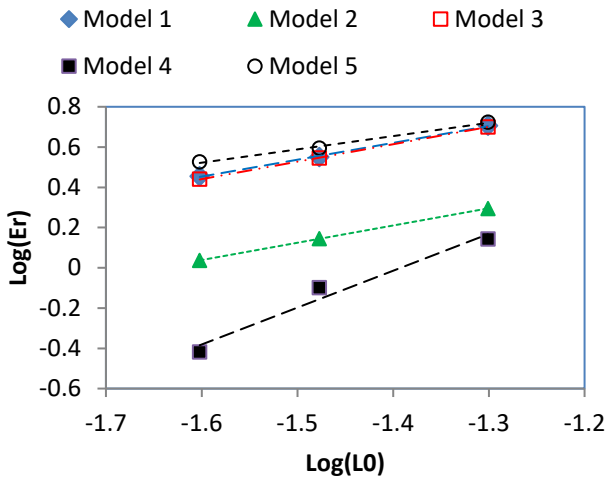

Fig. 2: Errors of the Laplacian models for the solution of equation (33).

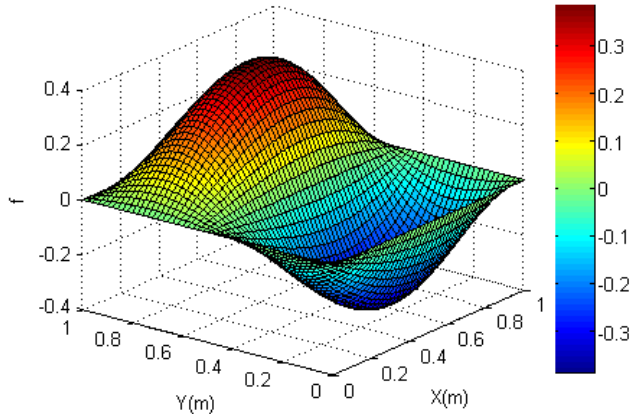

Fig. 3: Numerical solution of equation (33) using Model 2 with $L_0 = 1/40$ m.

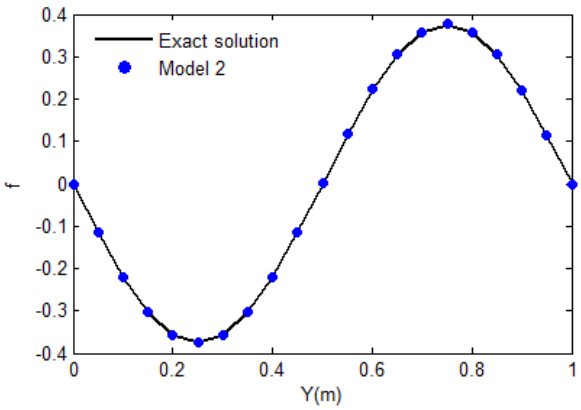

Fig. 4: Numerical result of equation (33) along $x = 0.5$ m using Model 2 with $L_0 = 1/40$ m.

A second numerical case study (equation (34)) was solved on the computational domain of figure 1 with $L_0 = 1/20$ m, $1/30$ m, $1/40$ m. For the solution of this equation, Models 1 and 3 were not considered in the error analysis due to their lower accuracy compared with the corresponding MLS-improve models. As seen in figure 5, Models 2 and 4 yielded smaller errors than Model 5, further showing the promising effects of incorporating the MLS shape functions into these models to get very high accuracy levels. Figures 2 and 5 show that the MPS model coupled with the MLS method could achieve the smallest errors among the presented models. From these figures, the convergence rates of all models are almost the same (less than 1) while Model 4 shows a higher rate (more than 1) for the solution of the first PDE (equation (33)). This can be explained by the fact that the numerical results depend to some extent on the high irregularity of the randomly generated node distributions (See figure 1) and the rate may change slightly in different numerical runs. Also, the type of differential equations can be effective on the convergence rate. It is expected higher rate can be achieved for more regular node configurations. Furthermore, a more accurate imposition of boundary conditions has a direct influence on this parameter. Figure 6 shows the solution of this PDE, in the form of contours, from Model 4 with $L_0 = 1/40$ m. The close agreement between the results of this model and the exact solution along $y = 0.5$ m is illustrated in figure 7, indicating the very high accuracy of Model 4.

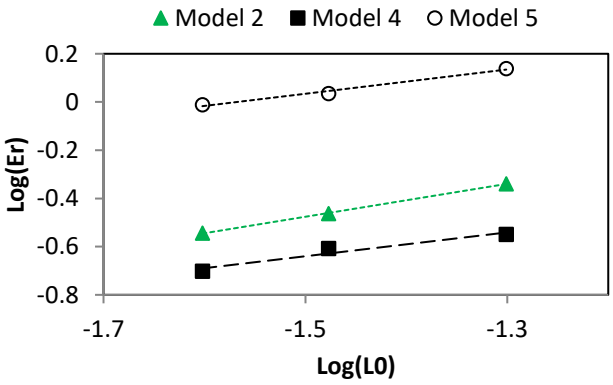

Fig. 5: Errors of the Laplacian models for solving equation (34).

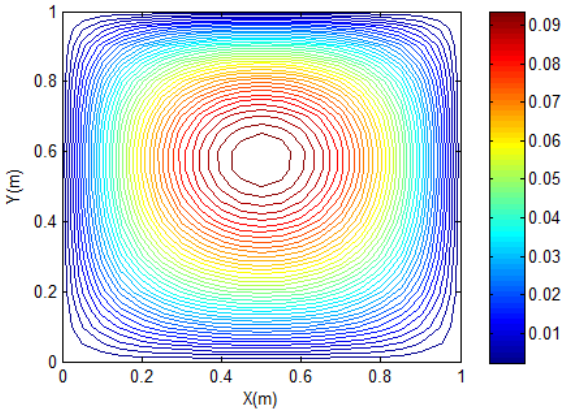

Fig. 6: Numerical solution of equation (34) using Model 4 with $L_0 = 1/40$ m.

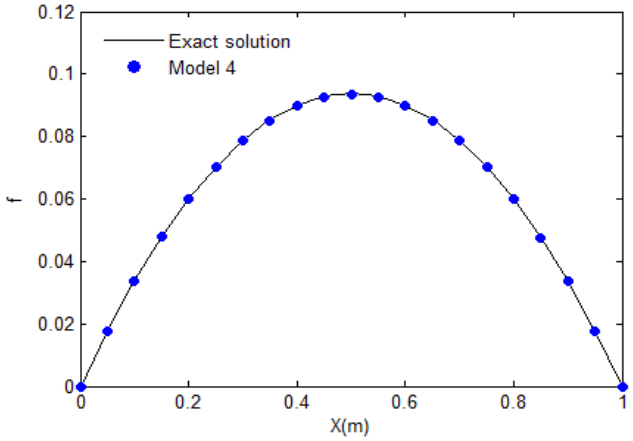

Fig. 7: Numerical result of equation (34) along $y = 0.5$ m using Model 4 with $L_0 = 1/40$ m.

To further examine the accuracy evaluation of the introduced models, two more complex non-geometric computational domains discretized with irregular node distributions corresponding to $L_0 = 1/40$ m, as shown in figures 8 and 9, respectively, were employed for solving equation (35). Figure 10 graphically demonstrates the errors for different models and node configurations, indicating the superior accuracy of Model 4. The color map of figure 11 further depicts the numerical solution of this model. Figure 12 compares the numerical results with the analytical solution along $y = 0.8$ m, indicating the high precision of Model 4. Similar to figures 11 and 12, Figures 13 and 14 display the results for the node distribution shown in figure 9, further demonstrating the notable performance of Model 4.

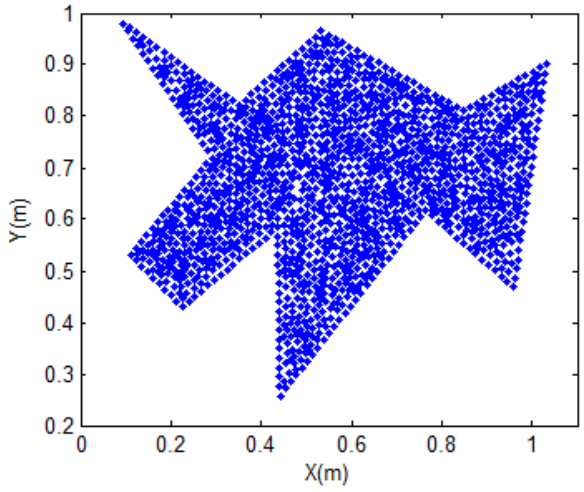

Fig. 8: The first node distribution with $L_0 = 1/40$ m for solving equation (35).

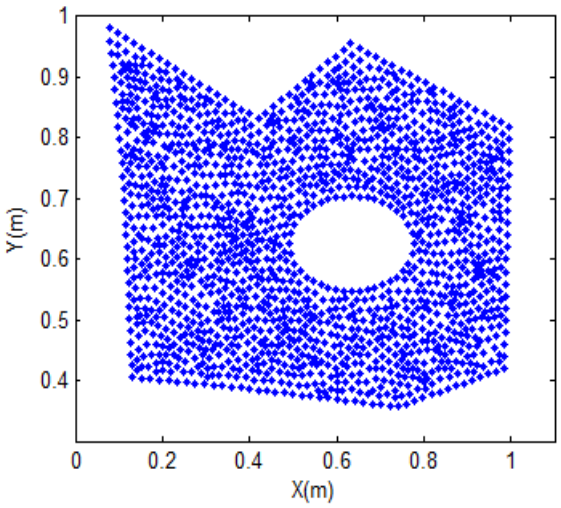

Fig. 9: The second node distribution with $L_0 = 1/40$ m for solving equation (35).

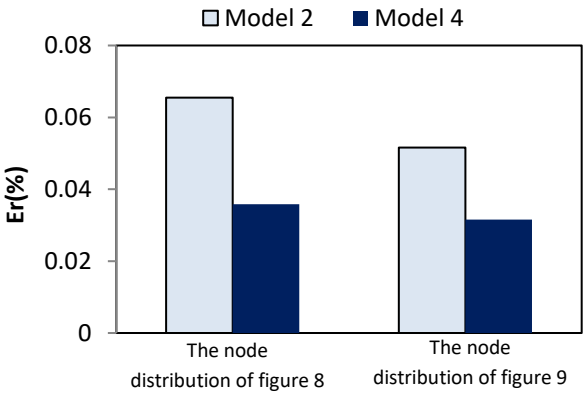

Fig. 10: Error of the proposed models for solving equation (35).

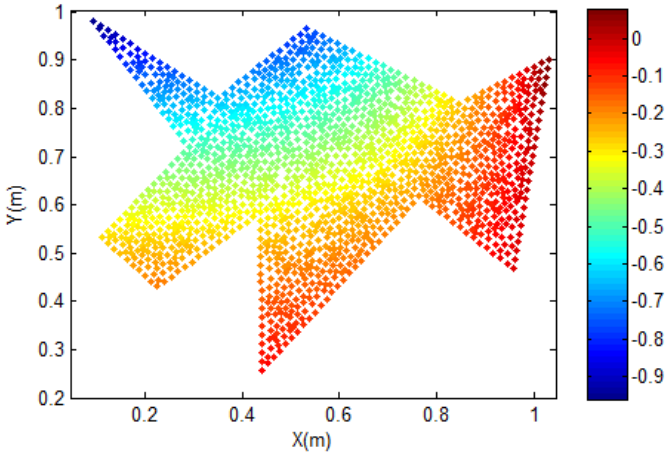

Fig. 11: Solution of equation (35) by Model 4 with the node distribution shown in Fig. 8.

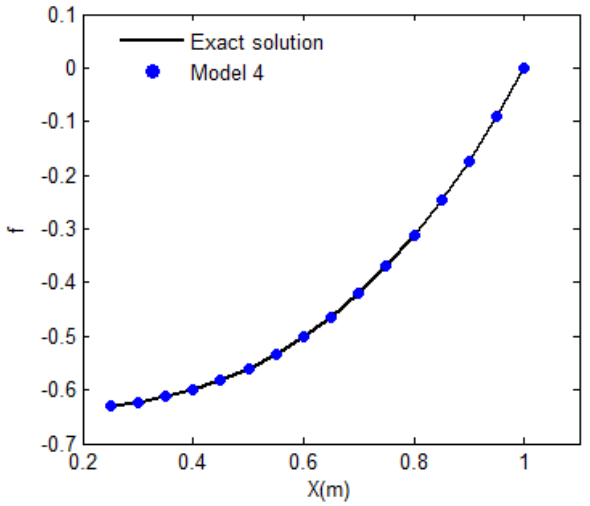

Fig. 12: Numerical result of equation (35) along $y = 0.8$ m using Model 4 for the node distribution of Fig. 8.

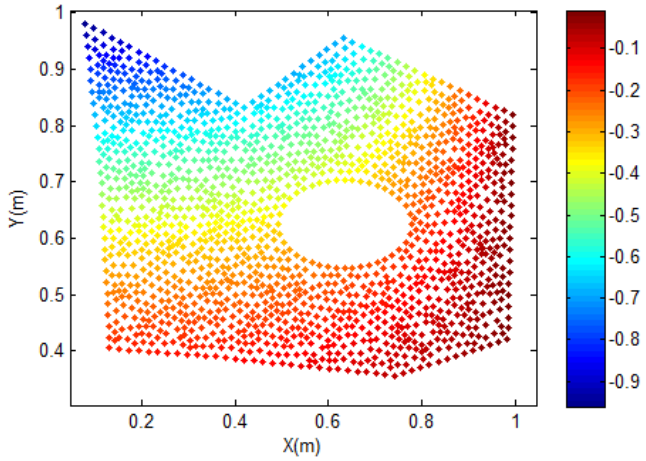

Fig. 13. The solution of equation (35) by Model 4 with the node distribution shown in figure 9.

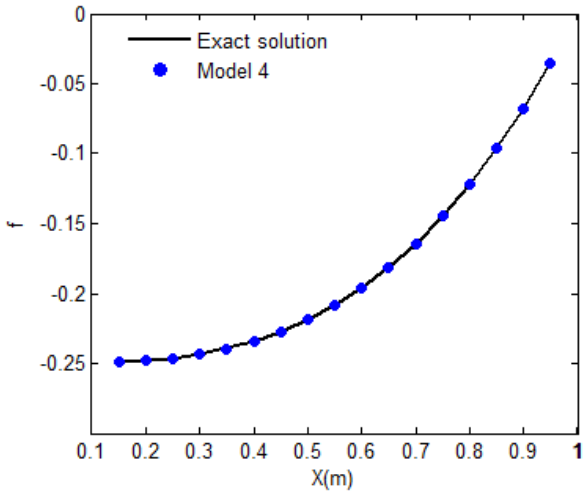

Fig. 14: Numerical result of equation (35) along $y = 0.5$ m using Model 4 for the node distribution shown in figure 9.

As a final case study (equation (36)), a PDE with a highly oscillatory solution was considered. Obtaining highly accurate results for such a PDE is a known challenge for numerical analysis. A fine node distribution with $L_0 = 1/100$ m (see figure 15) was used to evaluate the proposed models in this final case study. Figure 16 graphically demonstrates the errors produced by the proposed models, exhibiting better results from Model 4. Figure 17 depicts the numerical results obtained by Model 4, indicating significant periodic behavior of the solution. As seen in Figure 18, Model 4 produces very accurate results compared with the analytical solution along $y = 0.5$ m demonstrating promising capability of the scheme.

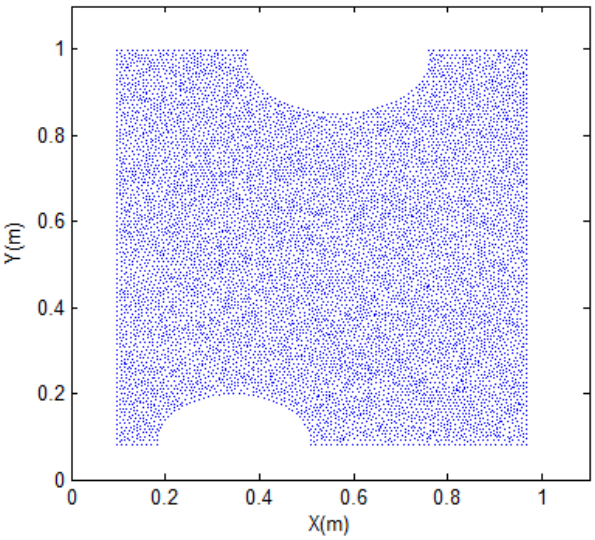

Fig. 15: The considered node distribution for solving equation (36) with $L_0 = 1/100$ m.

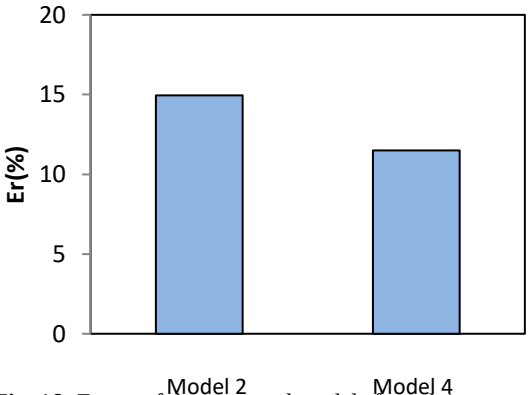

Fig. 16: Errors of the proposed models for solving equation (36).

4. Conclusion

As newly developed Laplacian models, the improved SPH and MPS methods [39, 40] were improved by MLS shape functions to achieve promising accuracy in solving Poisson equations encountered in 2D problems. The MLS shape functions replaced the weight functions applied in the original improved models. The realized enhancement in accuracy was a result of addressing an inherent deficit of

conventional weight functions near the boundaries of calculation domains. Previously, this deficit was resolved by using dummy particles beyond the boundaries. However, applying the MLS model for function approximation in this study eliminated the need for the dummy nodes. The superior accuracy of the proposed models over not only their original forms but also a widely used mixed model to reduce the order of PDEs was validated by solving different numerical case studies. The proposed schemes can be further developed to study more complex real-world problems encountered in solid and fluid mechanics.

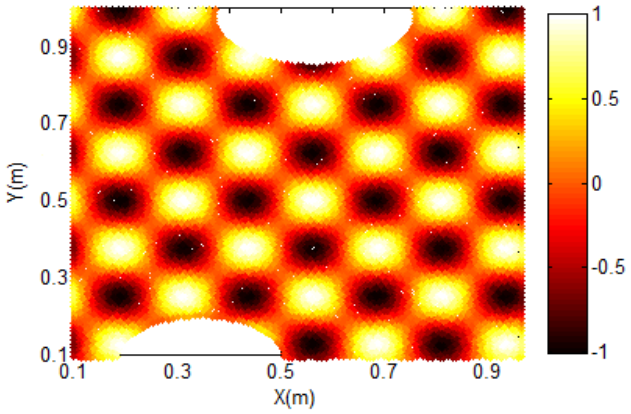

Fig. 17: The solution of equation (36) by Model 4.

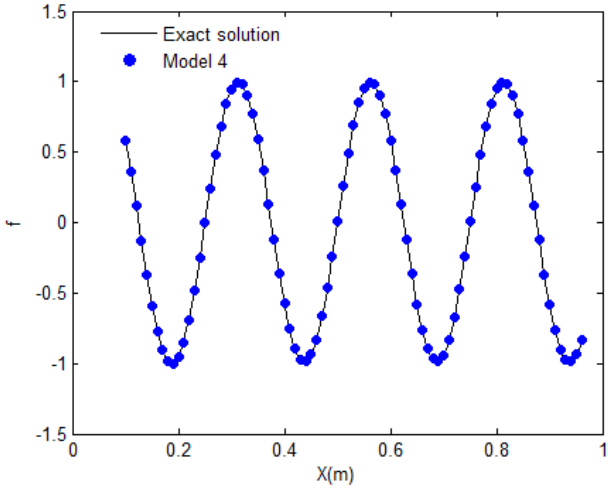

Fig. 18: Numerical result of solving equation (36) using Model 4 along $y = 0.5$ m.

Declarations

Conflict of interest The author declares no conflict of interest.

References

[1] Gingold, R. A., & Monaghan, J. J. (1977). Smoothed particle hydrodynamics: theory and application to non-spherical stars. Monthly notices of the royal astronomical society, 181(3), 375-389.

[2] Koshizuka, S., & Oka, Y. (1996). Moving-particle semi-implicit method for fragmentation of incompressible fluid. Nuclear science and engineering, 123(3), 421-434.

[3] Ataie-Ashtiani, B., & Shobeyri, G. (2008). Numerical simulation of landslide impulsive waves by incompressible smoothed particle hydrodynamics. International Journal for numerical methods in fluids, 56(2), 209-232.

[4] Shao, S. (2010). Incompressible SPH flow model for wave interactions with porous media. Coastal Engineering, 57(3), 304-316.

[5] Liu, X., Xu, H., Shao, S., & Lin, P. (2013). An improved incompressible SPH model for simulation of wave–structure interaction. Computers & Fluids, 71, 113-123.

[6] Liang, D., Jian, W., Shao, S., Chen, R., & Yang, K. (2017). Incompressible SPH simulation of solitary wave interaction with movable seawalls. Journal of Fluids and Structures, 69, 72-88.

[7] Ng, K. C., Ng, Y. L., Sheu, T. W. H., & Alexiadis, A. (2020). Assessment of Smoothed Particle Hydrodynamics (SPH) models for predicting wall heat transfer rate at complex boundary. Engineering Analysis with Boundary Elements, 111, 195-205..

[8] Zago, V., Bilotta, G., Hérault, A., Dalrymple, R. A., Fortuna, L., Cappello, A., ... & Del Negro, C. (2018). Semi-implicit 3D SPH on GPU for lava flows. Journal of Computational Physics, 375, 854-870.

[9] Wu, J., Zhang, G., Sun, Z., Yan, H., & Zhou, B. (2023). An improved MPS method for simulating multiphase flows characterized by high-density ratios and violent deformation of interface. Computer Methods in Applied Mechanics and Engineering, 412, 116103.

[10] Pan, X. J., Zhang, H. X., & Lu, Y. T. (2008). Numerical simulation of viscous liquid sloshing by moving-particle semi-implicit method. Journal of Marine Science and Application, 7(3), 184-189.

[11] Shibata, K., Koshizuka, S., Sakai, M., & Tanizawa, K. (2012). Lagrangian simulations of ship-wave interactions in rough seas. Ocean Engineering, 42, 13-25.

[12] Sun, Z., Chen, X., Xi, G., Liu, L., & Chen, X. (2017). Mass transfer mechanisms of rotary atomization: A numerical study using the moving particle semi-implicit method. International Journal of Heat and Mass Transfer, 105, 90-101.

[13] Liu, X., Xu, Y., Wang, K., Cheng, S., & Tong, L. (2024). Study on bubble dynamics in sodium using three-dimensional MPS method. Nuclear Engineering and Design, 416, 112810.

[14] Liu, M. B., & Liu, G. R. (2006). Restoring particle consistency in smoothed particle hydrodynamics. Applied numerical mathematics, 56(1), 19-36.

[15] Oger, G., Doring, M., Alessandrini, B., & Ferrant, P. (2007). An improved SPH method: Towards higher order convergence. Journal of Computational Physics, 225(2), 1472-1492.

[16] Schwaiger, H. F. (2008). An implicit corrected SPH formulation for thermal diffusion with linear free surface boundary conditions. International journal for numerical methods in engineering, 75(6), 647-671.

[17] Shao, J. R., Li, H. Q., Liu, G. R., & Liu, M. B. (2012). An improved SPH method for modeling liquid sloshing dynamics. Computers & Structures, 100, 18-26.

[18] Jiang, T., Ouyang, J., Ren, J. L., Yang, B. X., & Xu, X. Y. (2012). A mixed corrected symmetric SPH (MC-SSPH) method for computational dynamic problems. Computer Physics Communications, 183(1), 50-62.

[19] Ikari, H., Khayyer, A., & Gotoh, H. (2015). Corrected higher order Laplacian for enhancement of pressure calculation by projection-based particle methods with applications in ocean engineering. Journal of ocean engineering and marine energy, 1, 361-376.

[20] Huang, C., Lei, J. M., Liu, M. B., & Peng, X. Y. (2016). An improved KGF-SPH with a novel discrete scheme of Laplacian operator for viscous incompressible fluid flows. International Journal for Numerical Methods in Fluids, 81(6), 377-396.

[21] Zhu, G. X., Zou, L., Chen, Z., Wang, A. M., & Liu, M. B. (2018). An improved SPH model for multiphase flows with large density ratios. International Journal for Numerical Methods in Fluids, 86(2), 167-184.

[22] Violeau, D., & Fonty, T. (2019). Calculating the smoothing error in SPH. Computers & Fluids, 191, 104240.

[23] Shobeyri, G. (2020). Accuracy analysis of different Laplacian models of incompressible SPH method improved by using Voronoi diagram. Journal of the Brazilian Society of Mechanical Sciences and Engineering, 42(10), 527.

[24] Heydari, Z., Shobeyri, G., & Ghoreishi Najafabadi, S. H. (2020). Accuracy analysis of different higher-order Laplacian models of Incompressible SPH method. Engineering Computations, 37(1), 181-202.

[25] Garoosi, F., & Shakibaeinia, A. (2020). An improved high-order ISPH method for simulation of free-surface flows and convection heat transfer. Powder Technology, 376, 668-696.

[26] Rajapriyadharshini, J. R. (2022). An improved smoothed particle hydrodynamics approach using new inverse kernel function. Journal of Ocean Engineering and Science, 7(4), 327-336.

[27] Gao, T., Liang, T., & Fu, L. (2023). A new smoothed particle hydrodynamics method based on high-order moving-least-square targeted essentially non-oscillatory scheme for compressible flows. Journal of Computational Physics, 489, 112270.

[28] Antuono, M., Sun, P. N., Marrone, S., & Colagrossi, A. (2021). The δ-ALE-SPH model: An arbitrary Lagrangian-Eulerian framework for the δ-SPH model with particle shifting technique. Computers & Fluids, 216, 104806.

[29] Rastelli, P., Vacondio, R., & Marongiu, J. C. (2023). An arbitrarily Lagrangian–Eulerian SPH scheme with implicit iterative particle shifting procedure. Computer Methods in Applied Mechanics and Engineering, 414, 116159.

[30] Khayyer, A., & Gotoh, H. (2009). IMPROVED MPS METHODS FOR WAVE IMPACT CALCULATIONS. In Proceedings Of Coastal Dynamics 2009: Impacts of Human Activities on Dynamic Coastal Processes (With CD-ROM) (pp. 1-14).

[31] Khayyer, A., & Gotoh, H. (2010). A higher order Laplacian model for enhancement and stabilization of pressure calculation by the MPS method. Applied Ocean Research, 32(1), 124-131.

[32] Sun, Z., Djidjeli, K., & Xing, J. T. (2015). Modified MPS method for the 2D fluid structure interaction problem with free surface. Computers & Fluids, 122, 47-65.

[33] Wang, L., Jiang, Q., Nie, S., Zhang, J., & Iddy, I. (2018). Improvement on MPS method for simulation of dynamic pressure in dam break flows. Journal of Coastal Research, (85), 971-975.

[34] Shobeyri, G., & Madadi, H. (2018). An improvement in MPS method using Voronoi diagram and a new kernel function. Journal of the Brazilian Society of Mechanical Sciences and Engineering, 40, 1-10.

[35] Jandaghian, M., Krimi, A., Zarrati, A. R., & Shakibaeinia, A. (2021). Enhanced weakly-compressible MPS method for violent free-surface flows: Role of particle regularization techniques. Journal of Computational Physics, 434, 110202.

[36] Yamada, D., Imatani, T., Shibata, K., Maniwa, K., Obara, S., & Negishi, H. (2022). Application of improved multiresolution technique for the MPS method to fluid lubrication. Computational Particle Mechanics, 9(3), 421-441.

[37] Matsunaga, T., & Koshizuka, S. (2022). Stabilized LSMPS method for complex free-surface flow simulation. Computer Methods in Applied Mechanics and Engineering, 389, 114416.

[38] Jian, L., Yu, P., Pei, J., Zeng, X., & Yuan, Y. (2022). Development of an MPS Code for Corium Behavior Analysis: 3D Alloy Melting. Science and Technology of Nuclear Installations, 2022(1), 2140729.

[39] Shobeyri, G. (2023). Using a modified MPS gradient model to improve accuracy of SPH method for Poisson equations. Computational Particle Mechanics, 10(5), 1113-1126.

[40] Shobeyri, G. (2024). Improved MPS models for simulating free surface flows. Mathematics and Computers in Simulation, 218, 79-97.

[41] Shao, S., & Lo, E. Y. (2003). Incompressible SPH method for simulating Newtonian and non-Newtonian flows with a free surface. Advances in water resources, 26(7), 787-800.

[42] Xu, R., Stansby, P., & Laurence, D. (2009). Accuracy and stability in incompressible SPH (ISPH) based on the projection method and a new approach. Journal of computational Physics, 228(18), 6703-6725.

[43] Zhang, S., Morita, K., Fukuda, K., & Shirakawa, N. (2006). An improved MPS method for numerical simulations of convective heat transfer problems. International journal for numerical methods in fluids, 51(1), 31-47.

[44] Duan, G., Yamaji, A., Koshizuka, S., & Chen, B. (2019). The truncation and stabilization error in multiphase moving particle semi-implicit method based on corrective matrix: Which is dominant?. Computers & Fluids, 190, 254-273.

[45] Liu, G. R. (2002). Meshfree methods: moving beyond the finite element method. CRC press.

[46] Faraji, S., Afshar, M. H., & Amani, J. (2014). Mixed discrete least square meshless method for solution of quadratic partial differential equations. Scientia Iranica, 21(3), 492-504.

[47] Eini, N., Afshar, M. H., Faraji Gargari, S., Shobeyri, G., & Afshar, A. (2020). A fully Lagrangian mixed discrete least squares meshfree method for simulating the free surface flow problems. Engineering with Computers, 1-21.

[48] Gargari, S. F., Kolahdoozan, M., Afshar, M. H., & Dabiri, S. (2019). An Eulerian–Lagrangian mixed discrete least squares meshfree method for incompressible multiphase flow problems. Applied Mathematical Modelling, 76, 193-224.

[49] Gargari, S. F., Huang, Z., & Dabiri, S. (2024). An upwind moving least squares approximation to solve convection-dominated problems: An application in mixed discrete least squares meshfree method. Journal of Computational Physics, 506, 112931.

[50] Frachon, T., Nilsson, E., & Zahedi, S. (2024). Stabilized Lagrange Multipliers for Dirichlet Boundary Conditions in Divergence Preserving Unfitted Methods. arXiv preprint arXiv:2408.10089.

[51] Afshar, M. H., Lashckarbolok, M., & Shobeyri, G. (2009). Collocated discrete least squares meshless (CDLSM) method for the solution of transient and steady-state hyperbolic problems. International journal for numerical methods in fluids, 60(10), 1055-1078.

[52] Wang, X., Ouyang, J., & Feng, Z. (2013). Local Kronecker delta property of the MLS approximation and feasibility of directly imposing the essential boundary conditions for the EFG method. Engineering Analysis with Boundary Elements, 37(7-8), 1021-1042.

[53] Li, X., & Wang, Q. (2016). Analysis of the inherent instability of the interpolating moving least squares method when using improper polynomial bases. Engineering Analysis with Boundary Elements, 73, 21-34.

[54] Dehghan, M., & Abbaszadeh, M. (2018). Interpolating stabilized moving least squares (MLS) approximation for 2D elliptic interface problems. Computer Methods in Applied Mechanics and Engineering, 328, 775-803.